Supplementary Information

A Direct Z-scheme Heterojunction g-C_3N_4/α-Fe_2O_3 Nanocomposite for Efficiently Degrade Polymer-containing Oilfield Sewage under Visible Light

Xinqing Zhang,[†, a,] Li Xia,[†, b,] Chao Liu,[c] Xiaobo Cheng,[c] and Zhi Yang[c]*

[a]. College of Petroleum Engineering, Xi'an Shiyou University, Xi'an 710065, China
[b].College of Chemistry and Materials Science, Northwest University, Xi'an 710127, China
[c]. No. 1 oil production plant, PetroChina Changqing Oilfield, Xi'an 710000, China

Author Contributions

†. These authors contributed equally to this work.

Corresponding authors:

Xinqing Zhang E-mail address: xqzhang5464@126.com

Materials and methods

Materials and Instruments

Materials. All starting materials, reagents and solvents used in experiments werecommercially available, high-grade purity materials and used without furtherpurification. Urea, Isopropanol (IPA, 95%), Nafion, and $FeCl_3$ (PPOA, >98.0%) were purchased from Aladdin; Sulfuric acid (H_2SO_4, 75%~80%), Ethanol (CH_3CH_2OH, 99%) and Sodium acetate (CH_3COONa) were purchased from Adams-beta.

Instruments. Zeta (ζ)-potential data were obtained using a Zeta sizer Nano-ZS (Malvern Instruments, U.K.), the NCs were dispersed in EtOH solutions. Powder XRD (Rigaku, Japan) results were recorded on a D/MAX-RB diffractometer. Morphological structures and microscopic details were evaluated by SEM (JSM-7500F, JEOL) and TEM (JEM-2100F, JEOL). To estimate the surface elemental composition and chemical states of the samples, XPS measurements were performed on an ESCALAB 250 Xi electron spectrometer (Thermo Scientific Corporation, USA). The UV–vis DRS were employed to investigate the optical properties of the samples on the Shimadzu UV 2550 UV–vis spectrometer. The evaluation of PL spectra was carried out using a Hitachi F-7000 fluorescence spectrophotometer under the excitation of 365 nm UV light source. The time-resolved PL spectroscopy was recorded on a FLS 920 spectrometer (Edinburgh Instruments) with a 345 nm laser as the light source.

Synthesis

Synthesis of g-C_3N_4 Nanosheets: The g-C_3N_4 nanosheets were obtained by exfoliation of bulk g-C_3N_4 in isopropanol (IPA) and water mixture solvent based on the previous work [1]. Typically, bulk g-C_3N_4 was synthesized by heating 10 g of urea in the muffle-furnace at 550 ℃ for 2 h. Subsequently, 300 mg of bulk g-C_3N_4 was dispersed into the mixture solvent of 100 mL IPA and 50 mL water by sonication for 2 h to obtain the g-C_3N_4 nanosheet suspension.

Synthesis of α-Fe_2O_3 Hexagonal Nanoplates: The α-Fe_2O_3 hexagonal nanoplates were fabricated based on the previous report [2]. Accordingly, 2.0 mmol of $FeCl_3$ was dissolved into a mixture solvent containing 20 mL of ethanol and 1.4 mL of water under vigorous magnetic stirring. After complete dissolution of the $FeCl_3$, 1.6 g of sodium acetate was added under continuous stirring. Subsequently, the homogenous solution was transferred into a 50 mL Teflon-lined vial sealed with stainless steel jacket and held at 180 ℃ for 12 h. The resulting precipitate was rinsed with DI water and ethanol several times, and dried at 80 ℃ overnight yielding the α-Fe_2O_3 hexagonal nanoplates.

Construction of α-Fe_2O_3/g-C_3N_4 Composites: The α-Fe_2O_3/g-C_3N_4 composites were prepared by an electrostatic self-assembly approach based on the previous report [3]. A certain amount of g-C_3N_4 nanosheet suspension was pipetted out from its original suspension, and then the pH value was adjusted to 6 by adding 0.2 M H_2SO_4 solution. Subsequently, different amounts of α-Fe_2O_3 powder were added into the above suspension under sonication of 0.5 h and a homogenous suspension was obtained after 4 h of stirring. Then, the solvents were removed by rotary evaporation. The resultant mixture powders were washed by DI water and methanol a few times and dried in the oven at 80 ℃ overnight. The obtained photocatalysts with different weight ratios were denominated as g-C_3N_4/α-Fe_2O_3 (3:1), g-C_3N_4/α-Fe_2O_3 (2:1), g-C_3N_4/α-Fe_2O_3 (1:1), g-C_3N_4/α-Fe_2O_3 (1:2) and g-C_3N_4/α-Fe_2O_3 (1:1), respectively.

Electrochemistry measurements.

All electrochemical measurements (photocurrent, the Mott–Schottky spots and EIS) were carried out with a CHI 660E electrochemical workstation via a conventional three-electrode system in a 0.2 M Na_2SO_4 aqueous solution (pH = 6.8). The working electrode was ITO glass plates coated with a catalyst slurry, the counter electrode was a platinum foil, and the reference electrode was a saturated Ag/AgCl electrode. The Mott-Schottky plots were also measured over an alternating current (AC) frequency

of 500 Hz, 800 Hz and 1000 Hz. These three electrodes were immersed in the 0.2 M Na_2SO_4 aqueous solution. Electrochemical impedance spectra (EIS) measurements were recorded over a frequency range of 100 kHz – 0.1 Hz with ac amplitude of 20 mV at 0 V, and 0.2 M Na_2SO_4 aqueous solution was used as the supporting electrolyte.

Preparation of the working electrode: 2 mg photocatalyst were dispersed in a mixed solution of 990 μL ethanol and 10 μL Nafion D-520 dispersion solutions to generate a homogeneous slurry. Subsequently, 200 μL of slurry was transferred and coated on ITO glass plates (1 cm × 2 cm) then dried at room temperature. The Ag/AgCl electrode was employed as the reference electrode, and platinum plate was used as the counter electrode, respectively.

Photocatalytic experiments

The photocatalytic activity of a sample was evaluated by degradation of HPAM solution under visible light irradiation. The solution was illuminated vertically using a 300-W Xe lamp (PLS-SXE300UV, Beijing Perfect Light Co., Ltd.) with a UV cut-off filter ($\lambda \geq 420$ nm). Degradation of HPAM was performed in a 100 mL glass reactor with an ice bath to maintain the solution at 0 °C. HPAM solution (50 mL, 30 $mg \cdot L^{-1}$) mixed with 10 mg photocatalyst was placed into the glass reactor. Before a photocatalytic measurement was carried out, the mixed solution was continuously stirred in dark condition for 60 min to achieve adsorption-desorption equilibrium. A sample used as a dark control was wrapped with aluminum foil and kept in dark environment. After the photocatalytic reaction starts, 3 mL of the suspension was taken every 20 minutes, and the concentration of HPAM was determined by spectrophotometer at a wavelength of 610 nm.

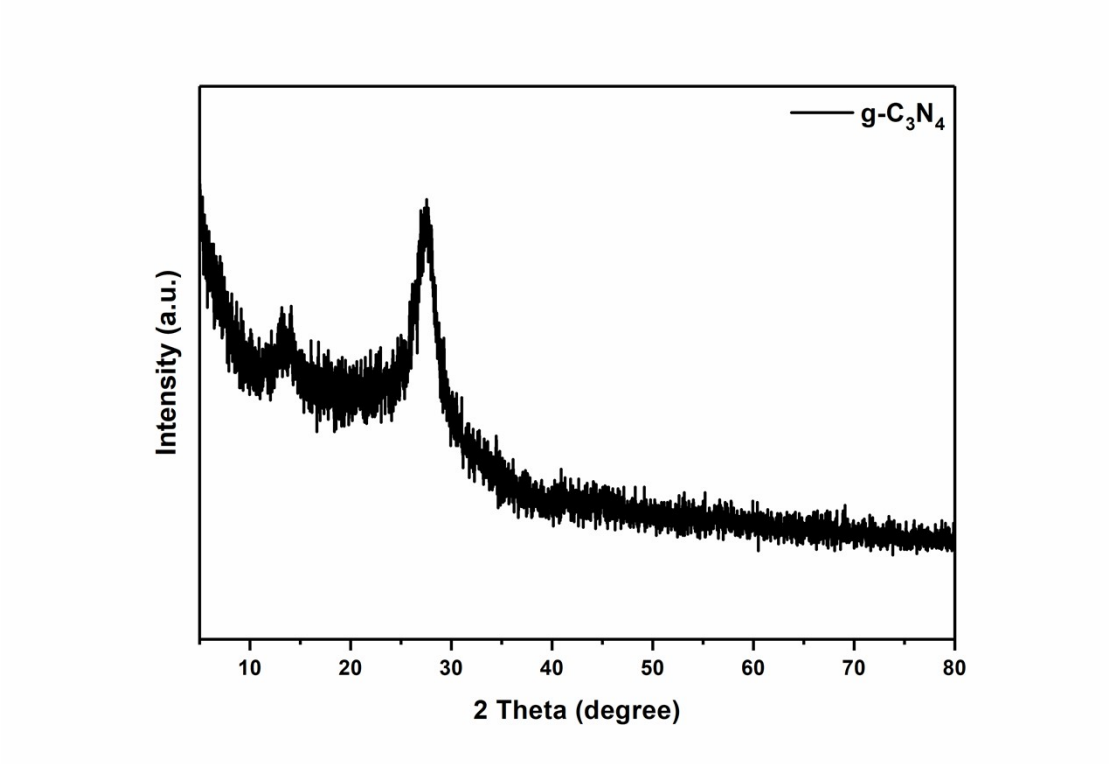

Figure S1. XRD of g-C_3N_4.

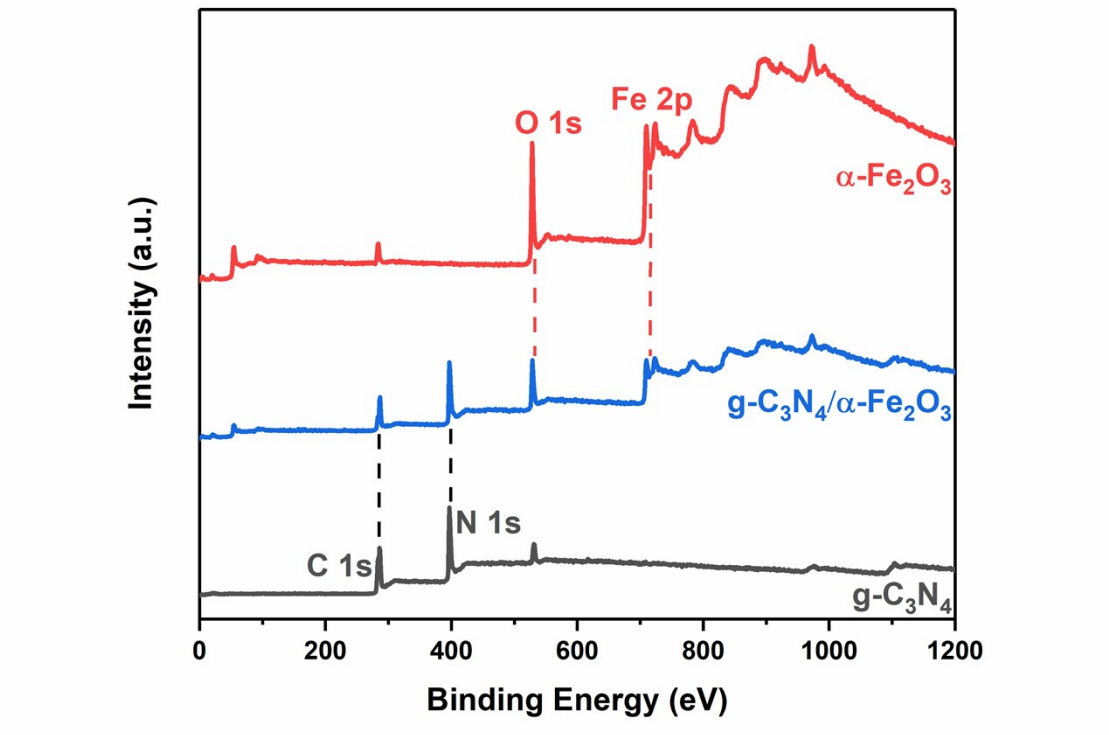

Figure S2. XPS survey spectrum of α-Fe_2O_3, g-C_3N_4 and g-C_3N_4/α-Fe_2O_3 (1:2).

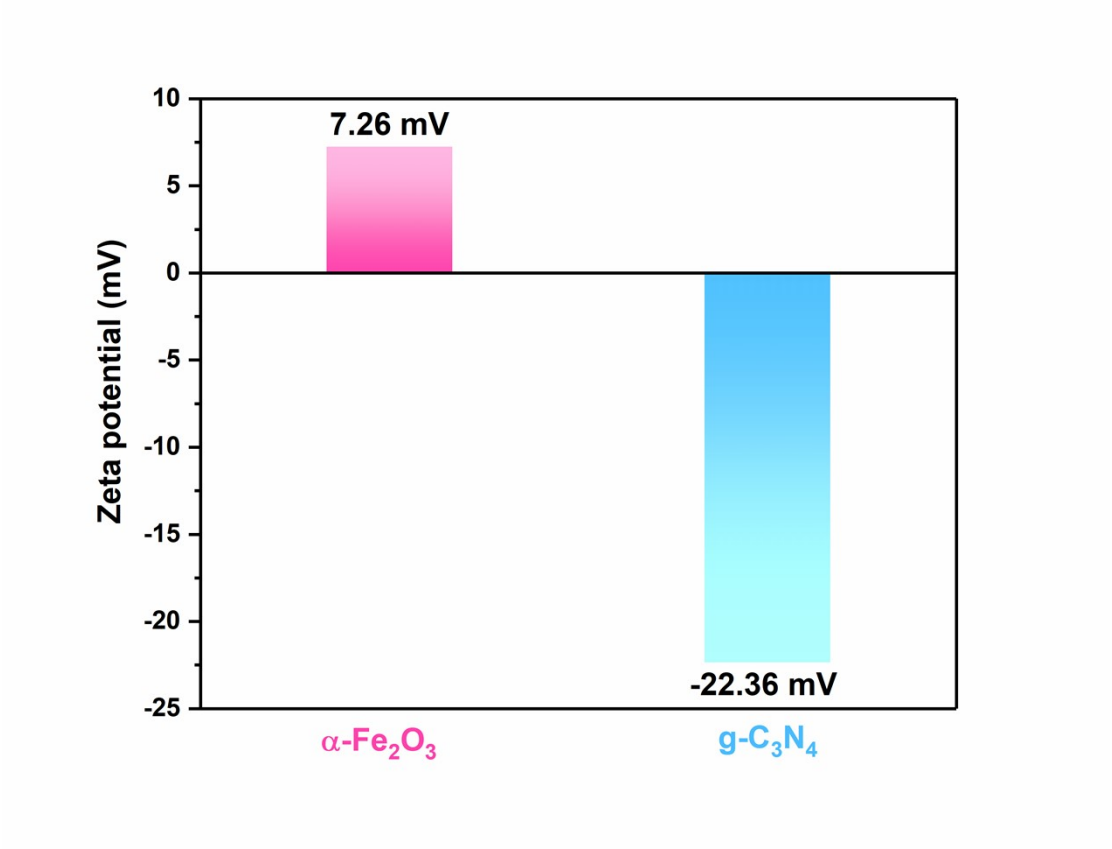

Figure S3. Zeta potential of g-C_3N_4 and Fe_2O_3 dispersed in DI water at pH = 6.

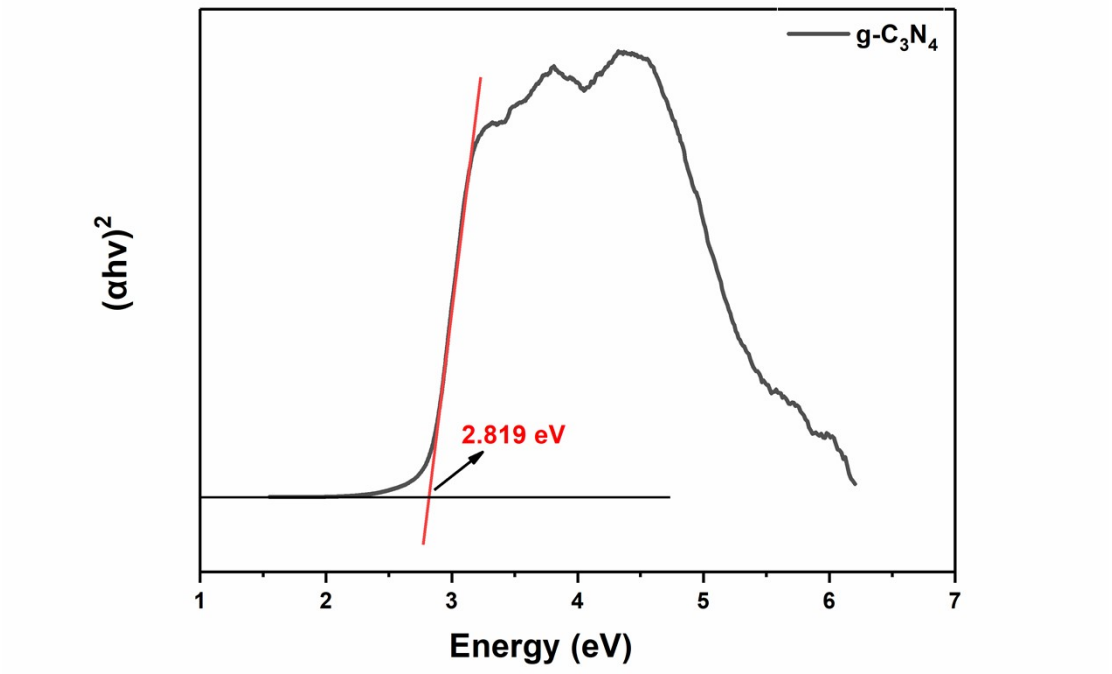

Figure S4. plots of $(Ahv)^2$ versus photon energy of g-C_3N_4.

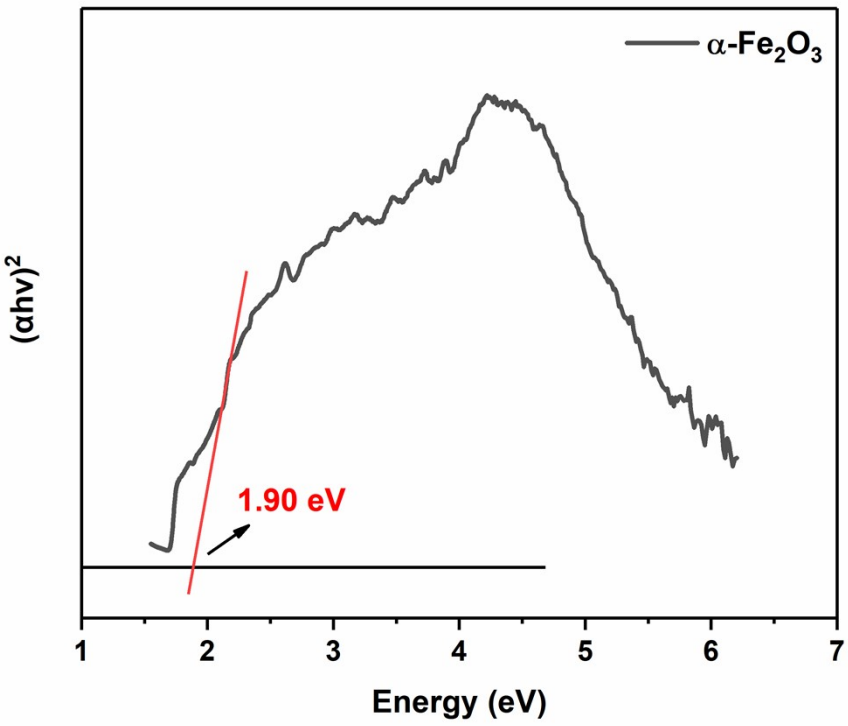

Figure S5. plots of $(Ahv)^2$ versus photon energy of α-Fe_2O_3.

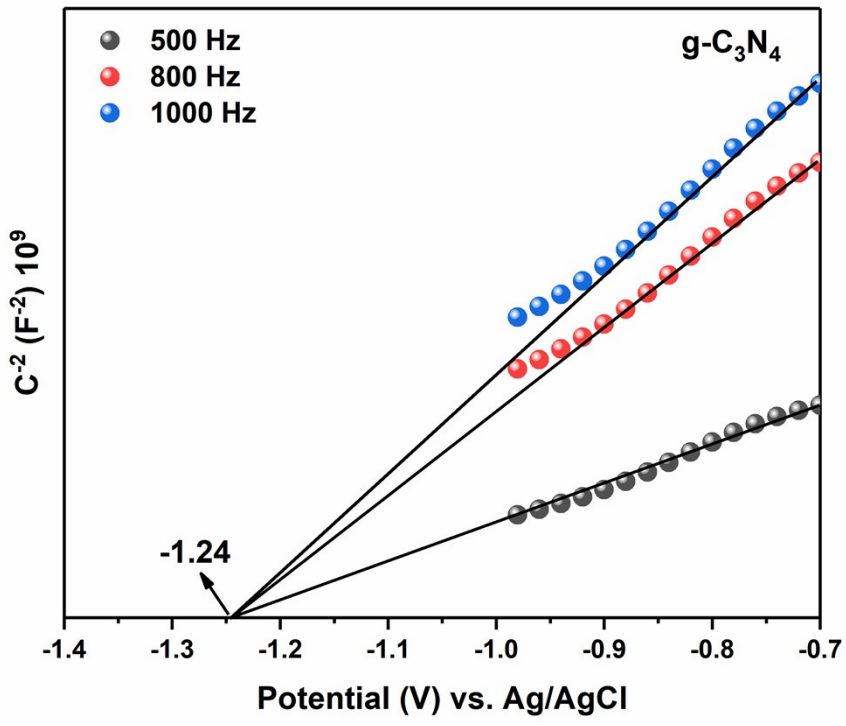

Figure S6. M-S plots of g-C_3N_4 samples.

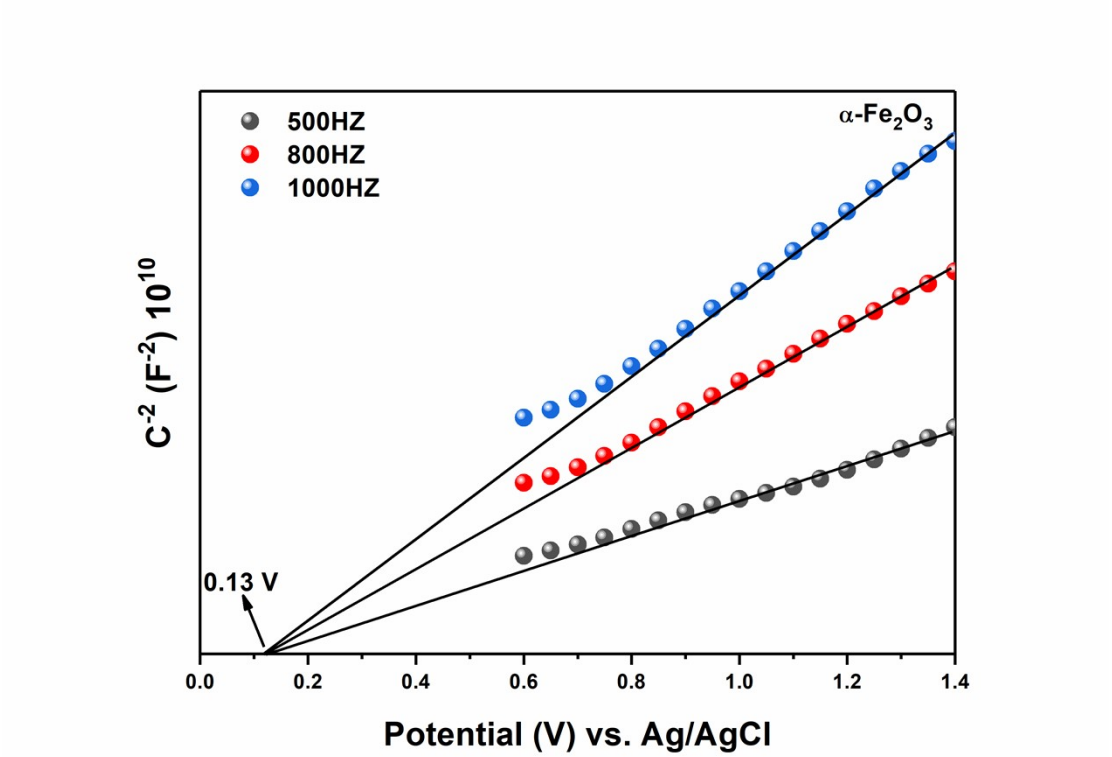

Figure S7. M-S plots of α-Fe_2O_3 samples.

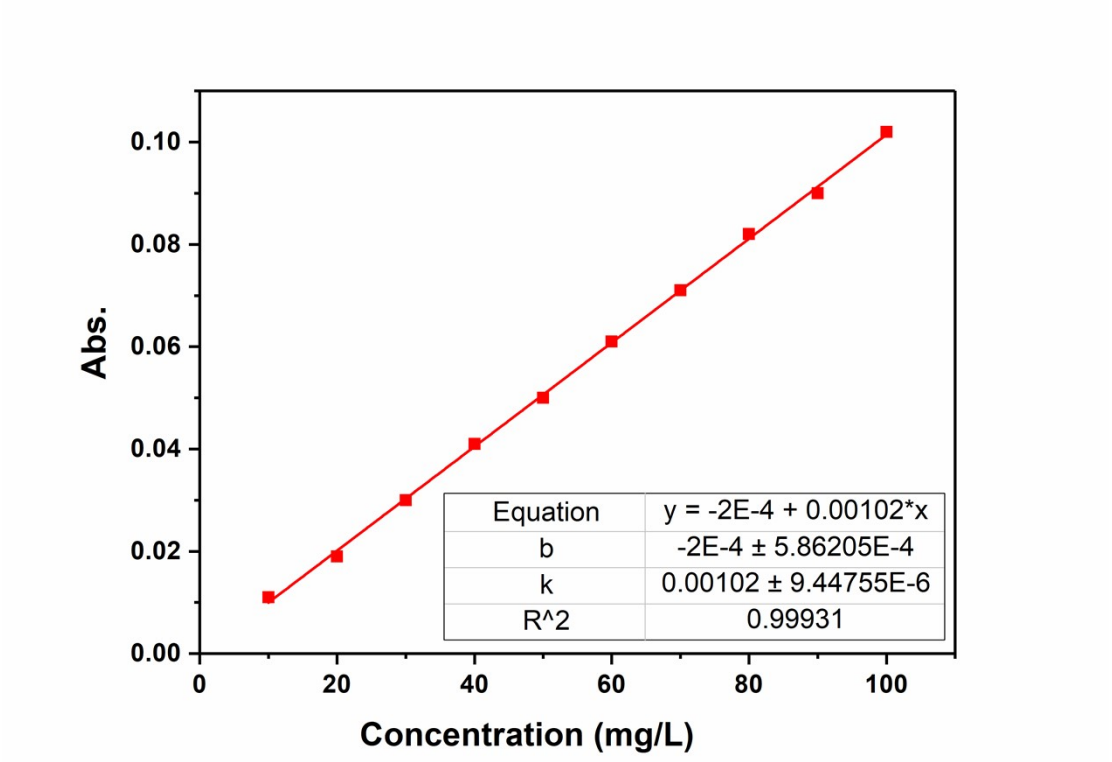

Figure S8. The standard curve of HAPM concentration.

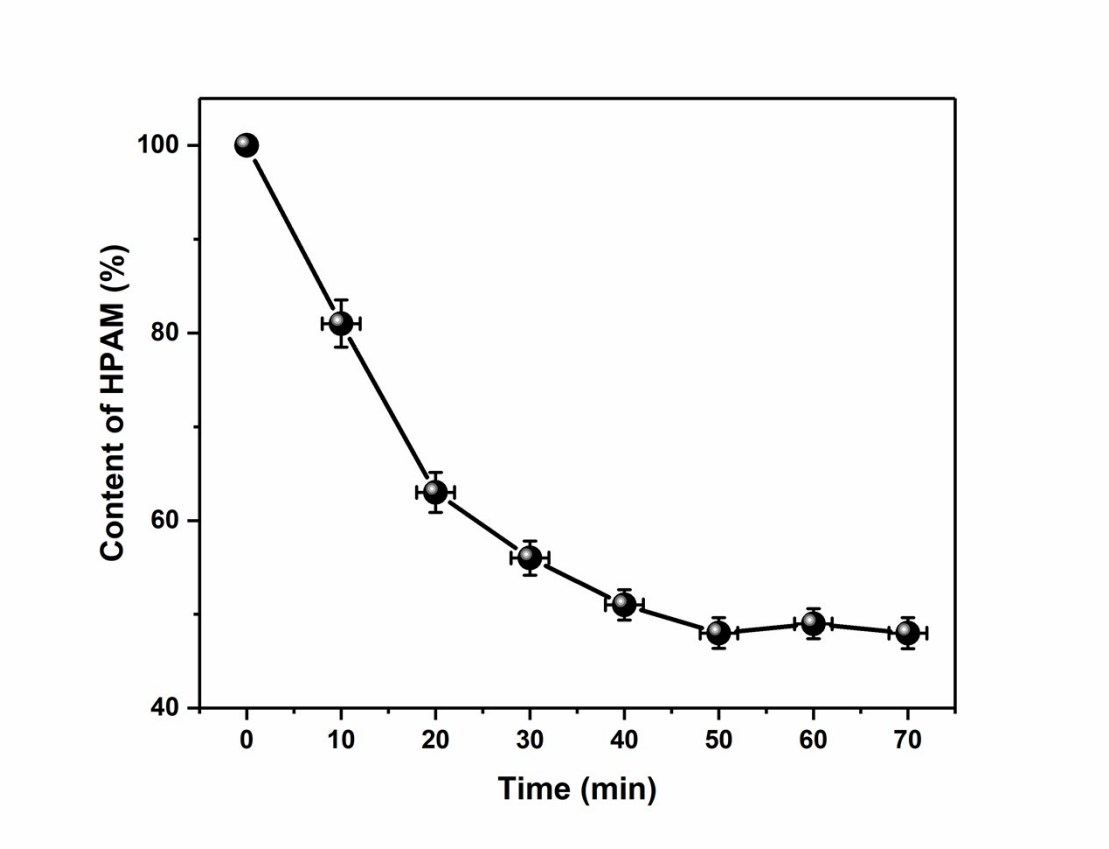

Figure S9. HPAM adsorption equilibrium test under dark conditions.

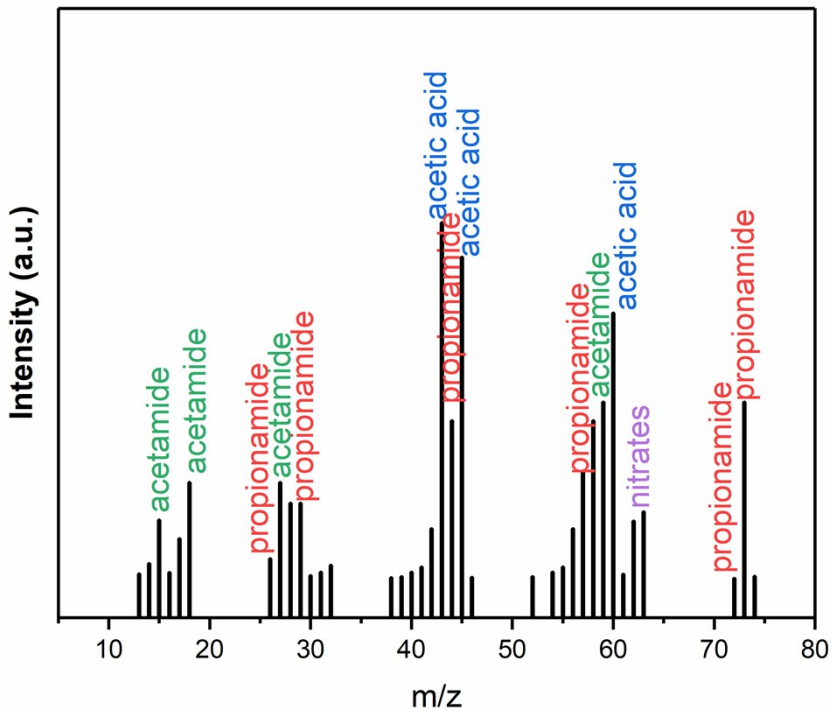

Figure S10. Mass spectrum of photocatalytically degraded HPAM under visible light irradiation showing detection of acetic acid, acetamide, propionamide and nitrate formed photocatalytic treatment as recorded using triple LC-MS.

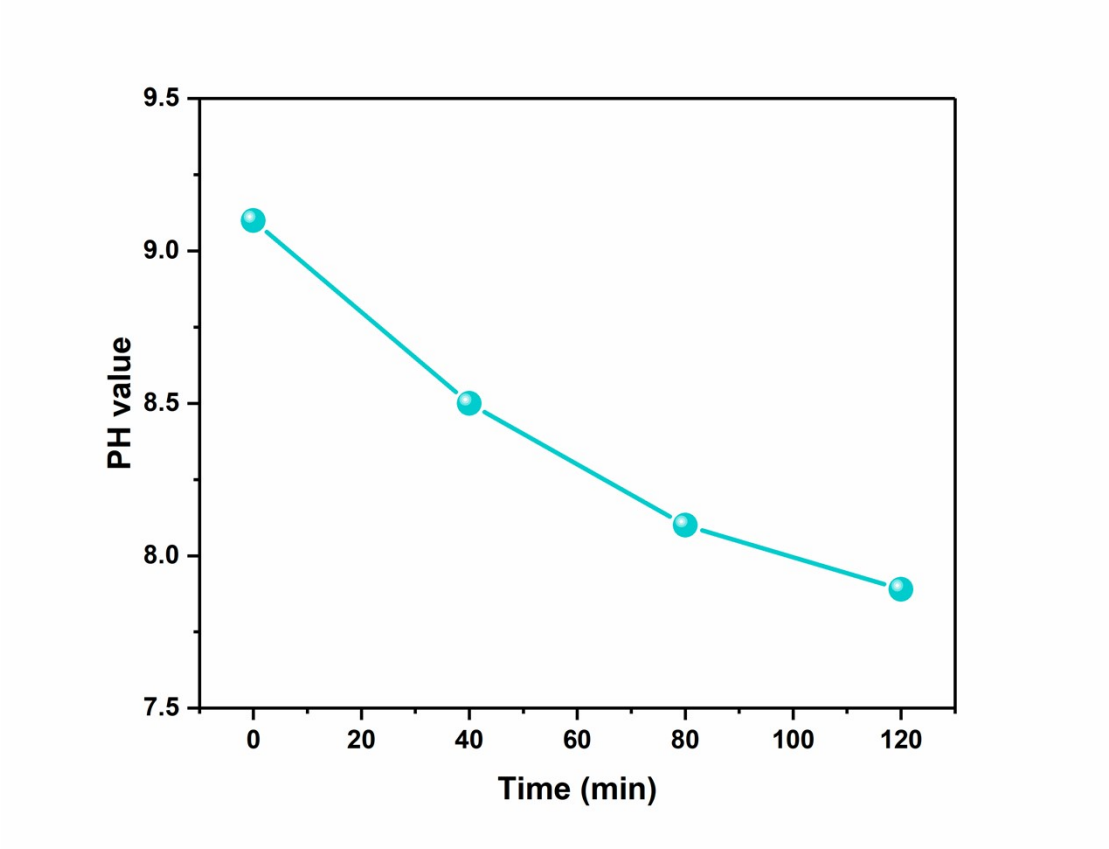

Figure S11. Change in pH of HPAM solution under visible light irradiation. The pH of the solution was measured at 40-minute time interval.

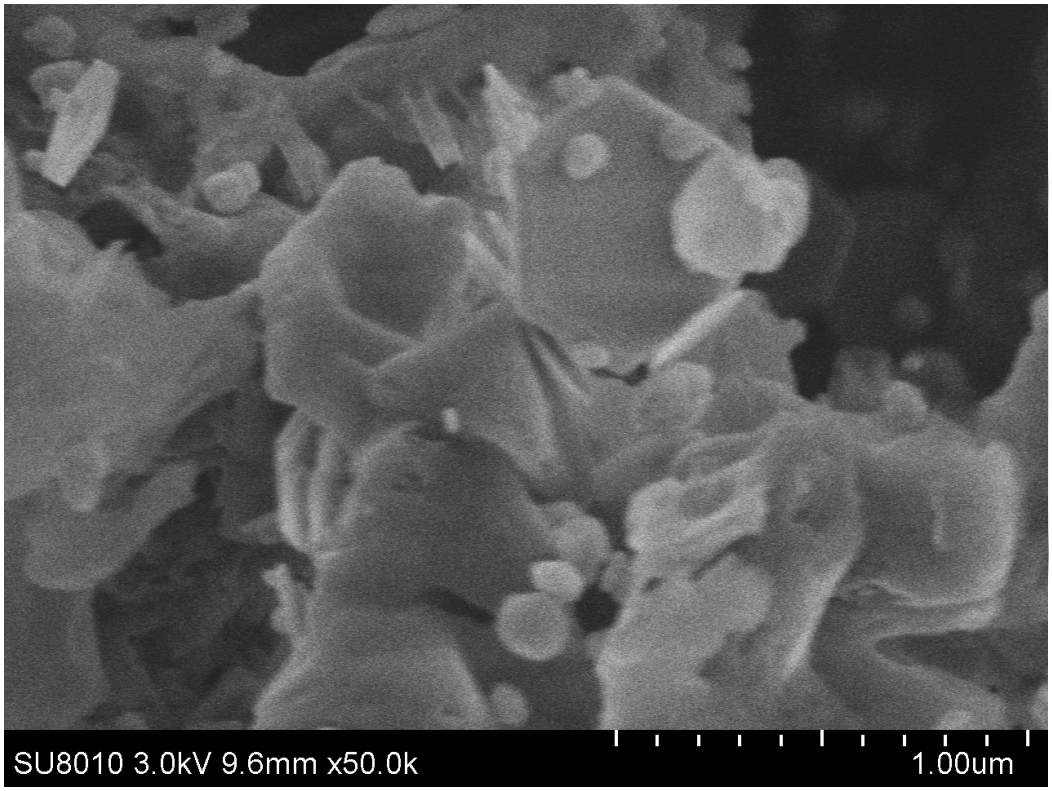

Figure S12. the SEM image of **g-C_3N_4/α-Fe_2O_3 (1:2)** after four times photocatalytic cycle.

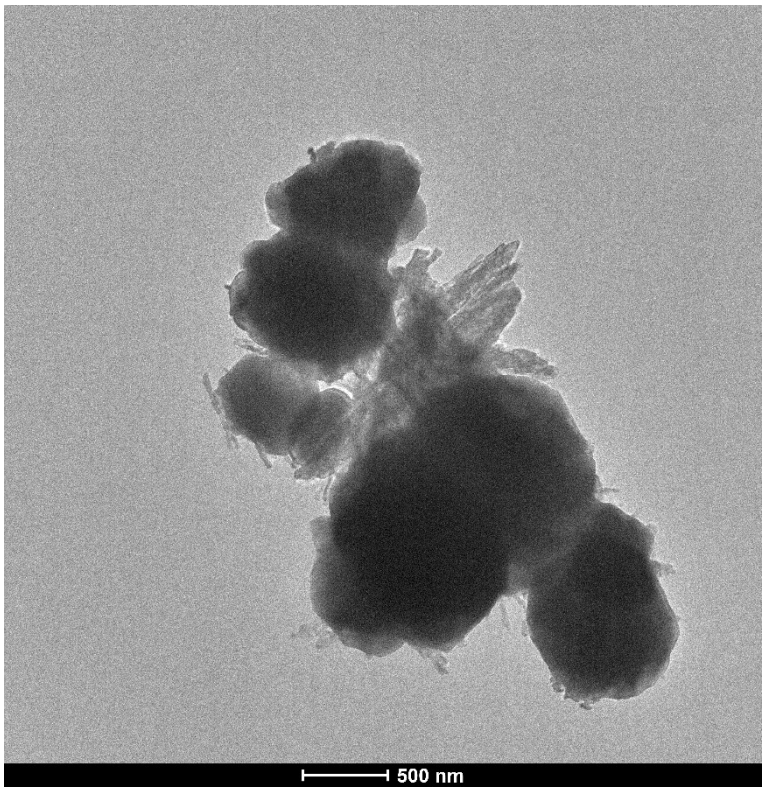

Figure S13. the TEM image of **g-C_3N_4/α-Fe_2O_3 (1:2)** after four times photocatalytic cycle.

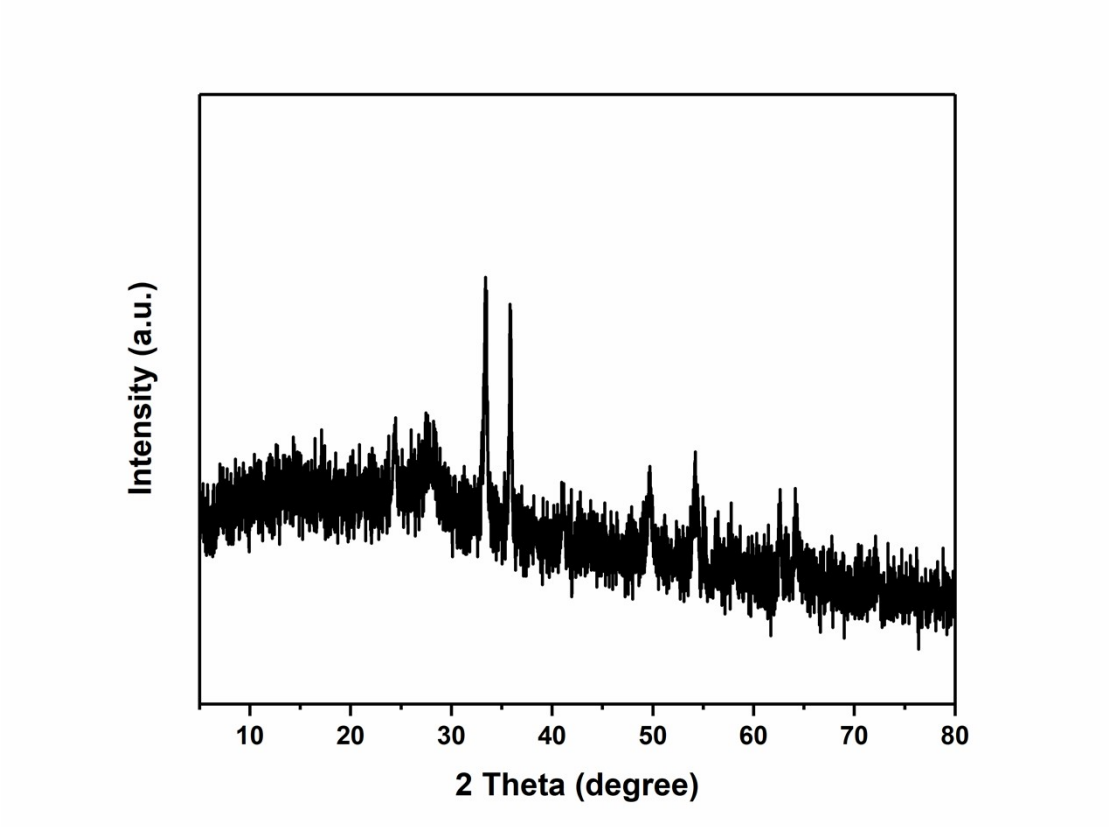

Figure S14. the XRD of **g-C_3N_4/α-Fe_2O_3 (1:2)** after four times photocatalytic cycle.

Table S1. The photocatalyst g-C_3N_4/α-Fe_2O_3 (1:2) degrades HPAM with 120 min light radiation under the different reaction conditions.

Comparative experiments	Reaction conditions	Degradation efficiencies
1	No photocatalyst	0.85 %
2	No light radiation	8.63 %
3	No photocatalyst and light radiation	-

Table S2. The apparent rate constant and the correlation coefficient (R^2) of the all the catalysts in the degradation of HPAM.

Catalysts	slope	R^2	K_{app} min^{-1}
g-C_3N_4	-0.00191	0.009836	0.00191
α-Fe_2O_3	-0.00282	0.009827	0.00282
g-C_3N_4/α-Fe_2O_3 (3:1)	-0.00371	0.009883	0.00371
g-C_3N_4/α-Fe_2O_3 (2:1)	-0.00547	0.009865	0.00547
g-C_3N_4/α-Fe_2O_3 (1:1)	-0.00864	0.009903	0.00864
g-C_3N_4/α-Fe_2O_3 (1:2)	-0.01747	0.009886	0.01747
g-C_3N_4/α-Fe_2O_3 (1:3)	-0.01194	0.009925	0.01194

Table S3. Summary of PL lifetime and electron transfer rate constant of samples fitted by double-exponential model.

Catalysts	**τ_1/ns**	**A_1 /%**	**T_2/ns**	**A_2 /%**	**<τ>/ns**
g-C_3N_4	1.62	40.3	6.88	59.7	4.76
g-C_3N_4/α-Fe_2O_3 (1:2)	2.39	41.2	11.48	58.8	7.74

The obtained decay profile can be reasonably fitted to a doubleexponential model:

$$< \tau > = (A_1{\tau_1}^2 + A_2{\tau_2}^2) / (A_1\tau_1 + A_2\tau_2)$$

where, $< \tau >$ is the average PL lifetime, τ_1 and τ_2 are the decay time constants, and A_1 and A_2 are the corresponding magnitudes.

Table S4. The apparent rate constant and the correlation coefficient (R^2) of the all the catalysts in the degradation of HPAM.

Photocatalysts	Process	Rate of degradation	Refences
g-C_3N_4/α-Fe_2O_3 (1:2)	Photocatalysis	90 %	This work
ZnO	Photocatalysis	74 %	Chemical Engineering Journal, 2018, 351, 56
Au/$BiVO_4$	Photocatalysis	80.37%	Industrial Water Treatment, 2021, 41, 74.
tBu-TPyzPzCo	Photoelectrocatalysis	94.55%	Catalysts 2021, 11, 181.
STSR	Photocatalysis	92.8%	Journal of Physics and Chemistry of Solids, 2021, 149, 109775
GCN/PAN	Photocatalysis	90.2%	Arabian Journal of Chemistry, 2020, 13, 4341
STT-700	Photocatalysis	88.2%	RSC Advanced, 2019, 9, 30790
Eu^{3+}/TiO2-2.4	Photocatalysis	83%	Applied Surface Science, 2009. 255, 3731
tBu-TPyzPzCo	Photoelectrocatalysis	94.55%	RSC Advanced, 2017, 7, 55496
Au/TiO_2	Photoelectrocatalysis	43.84%	RSC Advanced, 2016, 6, 63711

Reference

1. S. Yang, Y. Gong, J. Zhang, L. Zhan, L. Ma, Z. Fang, R. Vajtai, X. Wang and P. M. Ajayan, Exfoliated Graphitic Carbon Nitride Nanosheets as Efficient Catalysts for Hydrogen Evolution Under Visible Light, *Advanced Materials*, 2013, **25**, 2452-2456.
2. L. Chen, X. Yang, J. Chen, J. Liu, H. Wu, H. Zhan, C. Liang and M. Wu,

Continuous Shape- and Spectroscopy-Tuning of Hematite Nanocrystals, *Inorganic Chemistry*, 2010, **49**, 8411-8420.

3. Q. Xu, B. Zhu, C. Jiang, B. Cheng and J. Yu, Constructing 2D/2D Fe2O3/g-C3N4 Direct Z-Scheme Photocatalysts with Enhanced H2 Generation Performance, *Solar RRL*, 2018, **2**, 1800006.